Applied Surface Science 361 (2016) 122–132

Contents lists available at ScienceDirect

Applied Surface Science

journal homepage: www.elsevier.com/locate/apsusc

Potential of lattice Boltzmann to model droplets on chemically stripe-patterned substrates

H. Patrick Jansen, K. Sotthewes, Harold J.W. Zandvliet, E. Stefan Kooij*

Physics of Interfaces and Nanomaterials, MESA+ Institute for Nanotechnology, University of Twente, PO Box 217, 7500AE Enschede, The Netherlands

ARTICLE INFO

Article history:
Received 10 August 2015
Received in revised form
10 November 2015
Accepted 12 November 2015
Available online 18 November 2015

Keywords:
Directional wetting
Non-spherical droplets
Mumerical methods
Lattice Boltzmann modelling
Surface Evolver

ABSTRACT

Lattice Boltzmann modelling (LBM) has recently been applied to a range of different wetting situations. Here we demonstrate its potential in representing complex kinetic effects encountered in droplets on chemically stripe-patterned surfaces. An ultimate example of the power of LBM is provided by comparing simulations and experiments of impacting droplets with varying Weber numbers. Also, the shape evolution of droplets is discussed in relation to their final shape. The latter can then be compared to Surface Evolver (SE) results, since under the proper boundary conditions both approaches should yield the same configuration in a static state. During droplet growth in LBM simulations, achieved by increasing the density within the droplet, the contact line initially advances in the direction parallel to the stripes, therewith increasing its aspect ratio. Once the volume becomes too large the droplet starts wetting additional stripes, leading to a lower aspect ratio. The maximum aspect ratio is shown to be a function of the width ratio of the hydrophobic and hydrophilic stripes and also their absolute widths. In the limit of sufficiently large stripe widths the aspect ratio is solely dependent on the relative stripe widths. The maximum droplet aspect ratio in the LBM simulations is compared to SE simulations and results are shown to be in good agreement. Additionally, we also show the ability of LBM to investigate single stripe wetting, enabling determination of the maximum aspect ratio that can be achieved in the limit of negligible hydrophobic stripe width, under the constraint that the stripe widths are large enough such that they are not easily crossed.

1. Introduction

In the past years, considerable effort has been devoted to the experimental investigation of directional wetting on stripe-patterned surfaces [1–4]. It was shown that the final droplet shape not only depends on the surface pattern that is underneath the droplet, but also on the amount of kinetic energy that is involved in the deposition [5]. For a more detailed level of understanding, the ability to model and simulate the processes occurring in droplet deposition on such surfaces, an approach is required which enables accurate, realistic inclusion of kinetic effects. In this respect Lattice Boltzmann modelling (LBM) provides a powerful tool for this purpose. As compared to Surface Evolver (SE), a frequently employed package to calculate the minimum energy state of a droplet using a finite element approach, LBM has the major benefit that it does enable assessment of the kinetics leading to a final droplet shape. However, both methods should ultimately yield the same final droplet shape on a specific surface. Therefore we set out to benchmark the relatively new LBM approach applied to our experimental system, with results obtained using the more established SE method.

Kusumaatmaja et al. [6–8] studied the dynamics of droplets on chemically striped patterned surfaces, showing that different morphologies can exist, and that dynamics determine the droplet shape. They also showed the elongation of droplets on corrugated surfaces [9], both in experiment and in simulations. The elongation is strongly dependent on the amount of kinetic energy that is placed upon the droplet. David and Neumann applied free energy-minimizing simulations to confirm the agreement with experimental droplet shapes both on chemically striped [10] as well as grooved surfaces [11].

Wetting morphologies on chemically and topographically patterned surfaces have been studied by various groups [12–28]. For single stripe and channel/trench wetting, two different liquid morphologies exist: (i) the channel state and (ii) the bulge state. In the channel state the liquid only wets the hydrophilic stripe while being confined by the border between the hydrophilic and the

* Corresponding author.
E-mail address: e.s.kooij@utwente.nl (E.S. Kooij).
URL: http://www.utwente.nl/tnw/pin (E.S. Kooij).

http://dx.doi.org/10.1016/j.apsusc.2015.11.120
0169-4332/

hydrophobic stripe, or the morphologically structured part in the case of a trench. In the bulge state liquid starts to advance over the hydrophobic stripe or it starts to move outside the trench, resulting in a bulge at the center of the stripe. These studies show that the preferred state depends on the wettability of the stripes and the structures that are used. They do not focus on the maximum aspect ratio that can be achieved, which is one of the aspects we will deal with in this work.

As outlined above, in comparison to finite element approaches, LBM enables including kinetic effects [29]. Previously we performed a preliminary comparison between LBM and actual experiments [3]. Here we compare results obtained from LBM simulations to SE simulations, which allows us to place the same constraints on the droplet. As such, the SE results provide a benchmark to validate our LBM work.

After a description of the essential details of both numerical approaches, we first demonstrate the power and potential of LBM by a simulation of impacting droplets on stripe-patterned surfaces, and its effect on the final droplet shape. Since SE comprises a finite element approach, in which the energy of the droplet is continuously minimized, it does not allow taking into account kinetic effects such as they play a role in the example of impacting droplets. LBM on the other hand takes into account the full dynamics of the system and therewith allows a complete simulation revealing the kinetics as observed in actual experiments.

In the next section, we perform a more detailed analysis of final droplets shapes, comparing results of LBM and SE. In the case of the minimum energy state under the proper boundary conditions, both computational techniques should give the same results after the systems are left to relax to a stable, static situation. For both methods the aspect ratio is simulated as a function of α, where $\alpha = W_{dry}/W_{wet}$ is the ratio of the widths of dry (lyophobic) and wet (lyophilic) stripes, with contact angles set to $\theta_{dry} = 110^\circ$ and $\theta_{wet} = 40^\circ$. In addition, the wettability of the stripes is adjusted.

Finally, in the last section we again use LBM simulations to study droplet wetting on a single stripe. Since the temporal shape evolution is important, LBM allows us to discuss the up to now unanswered question what the maximum achievable aspect ratio of a droplet is.

2. Simulation details

2.1. Lattice Boltzmann

For the lattice Boltzmann modeling (LBM) simulations, we used the Shan-and-Chen-type multicomponent multiphase LBM [30]; for full details on the implementation of LBM we refer the reader to our previous work [3].

Two fluid components are modelled, each with its own distribution function. The lattice used for the simulations is always in 3D and is the D3Q19 lattice. The LBM model we used is described by Huang et al. [31]. The lattice Boltzmann equation used is given by:

$$f_i^\sigma(\mathbf{x} + \mathbf{e}_a\Delta t, t + \Delta t) = f_i^\sigma(\mathbf{x}, t) - \frac{\Delta t}{\tau_\sigma}[f_i^\sigma(\mathbf{x}, t) - f_i^{\sigma,eq}(\mathbf{x}, t)] \quad (1)$$

where $f_i^\sigma(x, t)$ is the distribution function of component σ (i.e. fluid 1 or fluid 2) in the ith velocity direction, and τ_σ is a relaxation time which is related to the kinematic viscosity by $\nu_\sigma = c_s^2(\tau_\sigma - 0.5)\Delta t$. The density of the fluid at a lattice site can be calculated by applying the following equation:

$$\rho_\sigma = \sum_{i=1}^{i} f_i^\sigma \quad (2)$$

where ρ_σ is the density of fluid 1 or 2 at a certain lattice site (lx, ly, lz). A single lattice site contains two densities where the minor components can be thought of as dissolved within the dominant component.

We typically have two forces acting on the fluids in our system: (i) the cohesion force and (ii) the adhesion force. No gravitational force is modeled, since the experimental volumes used are low enough for gravity to be neglected. The cohesion force holds the droplet together and determines the surface tension

$$\mathbf{F}_{c,\sigma} = -G_c\rho_\sigma(x, t)\sum_i w_i\rho_{\bar{\sigma}}(\mathbf{x} + \mathbf{e}_i\Delta t, t)e_i \quad (3)$$

where $\mathbf{F}_{c,\sigma}$ is the cohesion force for fluid 1 or 2, w_i is the weight parameter, and $\rho_{\bar{\sigma}}$ is the density of the opposite fluid. The strength of the cohesion force is determined by the parameter G_c. A low G_c value results in a mixing of the fluids and we end up with a single phase, while a higher G_c value induces a surface tension between the fluids thereby making them immiscible. The adhesion force is the force that a fluid particle experiences by being absorbed on the surface. This force can be described by

$$\mathbf{F}_{ads,\sigma} = -G_{ads,\sigma}\rho_\sigma(x, t)\sum_i w_i s(\mathbf{x} + \mathbf{e}_i\Delta t)\mathbf{e}_i \quad (4)$$

where the parameter G_{ads} determines the strength of the interaction. The location of the surface is indicated by s, and is 1 for surface node and 0 for a fluid node.

Following the work of Huang et al. [31], we can calculate the contact angle using

$$\cos(\theta_1) = \frac{G_{ads,2} - G_{ads,1}}{G_c\frac{\rho_1 - \rho_2}{2}} \quad (5)$$

where $G_{ads,1}$ is the adsorption constant for fluid 1 and $G_{ads,2}$ is the adsorption constant for fluid 2. Huang et al. found the most stable case when the adsorption constants are opposite to each other, i.e. $G_{ads,2} = -G_{ads,1}$.

To benchmark the adsorption energies, simulations were performed on a homogeneous surface at a specific adsorption energy. The parameters used in the simulation were $\rho_{air} = 0.06$ (density of the fluid 1), $\rho_{liquid} = 2.00$ (density of the fluid 2), $G_c = -0.87$ (cohesion parameter), $lx = 300$, $ly = 100$, $lz = 300$ (lattice sizes in the x, y, z-direction), $r = 40$ (radius of droplet in lattice units), $T_{max} = 15{,}000$ (number of time steps) and G_{ads} is varied.

To simulate a striped surface with varying wettability, four adsorption terms are used. Here we will make the distinction between a stripe that is wetted more than another, referred to as wet and dry stripes. Since we have two fluids, there are two adsorption terms for the wet stripe and two terms for the dry stripe. We apply an opposite adsorption energy for the two fluids, so only one adsorption energy will be mentioned for a certain stripe.

For the simulations presented in this work, a finite size of the simulation box requires definition of boundary conditions. At the sides of the simulation box we applied periodic boundary conditions [32], i.e. elements reaching the boundary appear on the opposite side. Simulations are accurate as long as care is taken that the droplet meniscus and therewith the three-phase contact line do not come too close to the edges. In other words, in practice this implies that the distance should be considerably larger that the diffusive layer thickness, which amount to 6 lattice units. On the top (liquid does not leave the system) and the bottom (liquid does not penetrate into the substrate) of the simulation volume the halfway bounce back boundary condition is applied in our simulations [33,34].

Finally, a general restriction in LBM simulations, which is attracting considerable attention nowadays, is that a direct connection between simulation parameters such as lattice units and time steps and actual experimental quantities such as distance and

time remains a major challenge. As such, our results are in all cases presented in terms of the simulation parameters.

2.2. Surface Evolver

Surface Evolver (SE) [35] is used to simulate the droplet shape on a chemically patterned surface, wetting 29 stripes as opposed to 7 for the LBM simulations. The SE procedures are identical to those used in our previous paper [36]; we briefly summarize details here. SE is a freely available software package, enabling the study of surfaces shaped by energies which are a combination of surface tension, gravitational energy, squared mean curvature, user-defined surface intergrals and/or knot energies. In SE a surface is implemented as a union of triangles formed by connecting vertices. Generally, the number of vertices can be increased for better accuracy of the shape. The surface is evolved toward its minimal energy by a gradient descent method in a number of iteration steps.

In our case, we only consider the surface tension of the liquid and the interaction with the substrate surface. In the simulations, gravity is ignored, since typical droplets in our experiments have a sufficiently small volume to neglect its influence. The equilibrium drop shape is obtained by a numerical procedure which minimizes the total free energy G of the droplet, which is given by

$$\frac{G}{\sigma_{lv}} = S_{lv} - \iint_{S_{sl}} \cos(\theta_i(x,y))dx\,dy \tag{6}$$

where σ_{lv} is the interfacial tension between the liquid and the vapor. S_{lv} and S_{sl} are the liquid–vapor and the solid–liquid interfacial areas of contact, and θ_i represents the intrinsic contact angle that generally depends on the position x and y on the substrate.

A typical substrate surface is divided into alternating stripes with high (hydrophobic) and low (hydrophilic) contact angles, already referred to as dry and wet stripes, respectively. The transition region is assumed to be sharp, i.e., we consider the modeled boundary between stripes as a step-function in surface energy and therewith a sharp discontinuity in contact angle. The intrinsic contact angle θ_i is defined by Youngs equation

$$\cos(\theta_i) = \frac{\sigma_{sv} - \sigma_{sl}}{\sigma_{lv}} \tag{7}$$

where σ_{lv}, σ_{sv} and σ_{sl} represent the interfacial tension between the liquid and the vapor, the solid and the vapor, and the solid and the liquid, respectively. Line tension is neglected in the simulations.

A volume of liquid is placed on the surface and is confined to stay on top of 29 stripes; if this restriction was not imposed, we encountered problems in evolving the droplet toward an equilibrium shape due to the fact that there is no gradient in energy between the different stripes. In that case, vertices do not have a specific direction to move along and started to move randomly resulting in a runaway of vertices. In order to avoid this effect, vertices are placed at the boundary between the stripes and confined to stay there. The initial shape of the liquid volume is that of a cube. Upon starting the iterations, the vertices of the droplet are moved in the direction prescribed by (i) the surface forces acting on them, (ii) a fixed volume constraint, and (iii) the constraint that the droplet has to be on the surface. This will continue until the total energy of the droplet no longer changes significantly. The surface is then refined for a more precise shape determination by adding additional vertices, and the iterations are recommenced. This procedure is repeated a number of times until the final refined equilibrium shape is reached. For a more detailed description of the technical procedure, we refer to the SE manual [35].

3. Demonstrating the power of LBM

3.1. Kinetic effects in impacting droplets

Before performing a detailed comparison between the two modelling approaches, we first demonstrate the potential of LBM by means of a simulation of impacting droplets on stripe-patterned surfaces. Recently, we presented an experimental study into the effect of kinetics on the final droplet shape on such chemically designed surfaces [5]. In the left panel of Fig. 1, the aspect ratio of droplets after impact on the surface is plotted as a function of the macroscopic hydrophobicity, expressed by the width ratio α of hydrophobic and hydrophilic stripes. The different coloured symbols represent experiments performed at different Weber numbers $We = \rho U_0^2 D_0/\sigma$, where ρ and σ are the density and surface tension of the liquid, respectively, U_0 the impact velocity and D_0 the initial diameter of the droplet. Droplets are jetted from an inkjet nozzle at a fixed speed of a few meters per second. The Weber number was varied by tuning the droplet volume; for the experiments in Fig. 1 the volume amounted to 80, 245 and 402 pL.

The Weber number compares the inertial force to the surface tension. When $We \gg 1$, the inertial force dominates the surface tension, emphasizing the role of impact kinetics. Clanet et al. [37] studied the maximum diameter of a droplet after impact on various surfaces. They concluded that the maximum diameter during the impact event scales as $D_{max}/D_0 \approx We^{1/4}$, independent of the surface wettability. This implies that for larger Weber numbers the maximum spreading diameter increases, and therewith the number of stripes crossed on a specific stripe pattern becomes larger.

The right part of Fig. 1 depicts two sets of snapshots from LBM simulations, for low (top) and high (bottom) Weber numbers, respectively. From the simulation it is immediately clear that the maximum spreading is in agreement with the aforementioned relation between We and D_{max}; for the low We situation only four hydrophilic stripes are covered, while in the case of the larger We up to six hydrophilic stripes are spanned by the droplet. Due to the energetically unfavourable retraction in the direction perpendicular to the stripes, as compared to the direction parallel to the stripes, the aspect ratio of the droplet after it comes to rest is affected by the inertia of the droplet, i.e. by the kinetics expressed by the Weber number. We stress that SE does not allow such kinetic modelling.

3.2. Shape evolution in LBM

The shape evolution of a growing droplet as a function of time is shown in Fig. 2 for an LBM simulation with absolute stripe widths of 10 lattice units (l.u.), for both stripes, i.e. $\alpha = 1.0$. Several snapshots are shown of the droplet at the liquid–solid interface (A–E), while the transients (F–G) depict the time evolution of the aspect ratio and the contact angles. (A) The droplet is deposited on the surface, starting as a sphere. (B) The droplet has spread over the surface, wetting 7 stripes. The density increase starts at the onset of the simulation; however this increase is small for short time scales so that the amount of added volume does not influence the motion of the droplet in the time that it is spreading. (C) Over time the volume of the droplet has increased substantially and the droplet has grown in the direction parallel to the stripes, therefore the aspect ratio of the droplet has increased. The contact angle in the parallel direction remains approximately constant with a value of 78°, while the contact angle in the perpendicular direction is increasing as a function of time. (D) The droplet has reached its maximum aspect ratio and the contact angle in the perpendicular direction has reached its maximum value. The droplet is bulging over the dry stripe, leading to an increase of its width. (E) The droplet has spread over the dry stripes and starts to fill the wet stripes, leading to a drop in the aspect ratio and in the perpendicular contact angle.

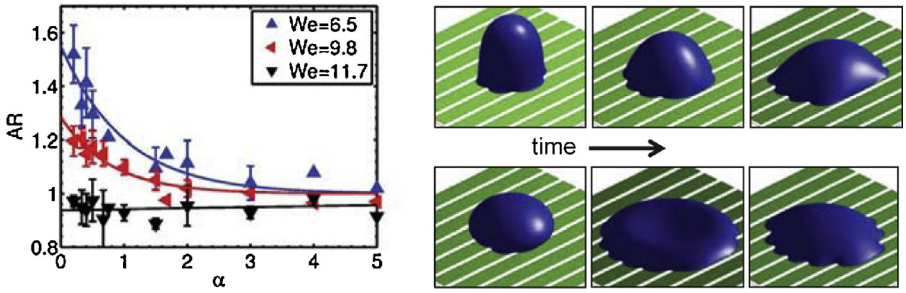

Fig. 1. (left) Aspect ratio as a function of α for droplets with different Weber numbers, deposited on stripe-patterned surfaces from an inkjet nozzle. Solid lines are a quide to the eye; adapted from [5]. (right) Subsequent snap-shots of LBM simulations of droplets with small (top) and large (bottom) Weber numbers.

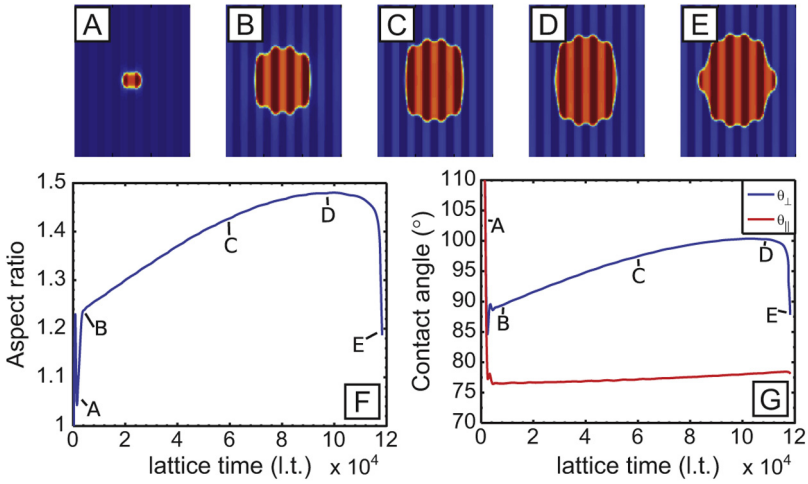

Fig. 2. (A–E) LBM simulation of the time evolution of a droplet shape at the solid–liquid interface. The dry stripes are the regions which appear brighter and the wet stripes are the regions that appear darker; red represents the droplet. The droplet is placed on the surface as a sphere, it spreads and subsequently grows due to the increase in density. Once the droplet becomes too large it spreads over the dry stripes wetting the next wet stripes. The time of the snapshots are indicated in (F) and (G) which show the aspect ratio and the contact angles as a function of time, respectively. (For interpretation of the references to color in this figure legend, the reader is referred to the web version of this article.)

Once the droplet has spread across the dry stripes the simulation is terminated. If the simulations were to be continued the droplet would again start to grow in the parallel direction, until it crosses the next dry stripes.

During its growth the droplet reaches its most elongated shape, which depends on the pattern underneath the droplet. The maximum aspect ratio corresponding to this state, i.e. the extremum in Fig. 2(G) is taken as the aspect ratio that can be achieved on a specific pattern. For the remainder of this paper when the aspect ratio is described as a function of the surface parameters, we refer to the maximum aspect ratio corresponding to those as in snapshot (D).

3.3. *Varying stripe widths and α for fixed wettabilities*

In Fig. 3 results are shown of LBM simulations with different stripe widths and fixed wettability of the stripes, i.e. $\theta_{wet} = 40^\circ$ and $\theta_{dry} = 110^\circ$. The aspect ratio (A) and the contact angles $\theta_\parallel$ and $\theta_\perp$ (B, C) are plotted as a function of α. These parameters are also plotted as a function of the absolute stripe width of the dry stripe, indicated by different colors and symbols as shown in the legend of the figure.

First we focus on the aspect ratio of the droplets shown in Fig. 3(A). The aspect ratios exhibit the same trend for various stripe widths, when compared to the experiments in previous work. For low α values the aspect ratio is high; spreading in the parallel direction is more favorable than spreading in the perpendicular direction giving rise to an elongated shape. As α increases the aspect ratio decreases and asymptotically approaches unity. There is however a clear difference between the various absolute stripe widths considered in the simulations. For an absolute dry stripe width of 1 lattice unit (l.u.) the aspect ratio is quite low; the maximum amounts to 1.2 for $\alpha = 0.04$ and a droplet is already spherical for $\alpha = 0.25$. As the absolute dry stripe widths are increased the aspect ratio also becomes higher, i.e. the overall curve rises to larger values. This upward trend continues as the dry stripe width is increased until the lines converge to a single curve for the largest stripe widths considered, i.e. 10–12 lattice units. The maximum aspect ratio achieved as a function of α is not highest for the largest stripe widths, since not all α values can be modeled. To reach low α values the wet stripe widths must be very large for wide dry stripes. The total width to wet 7 stripes is so large that the size of the lattice becomes too large, making the simulations slow and very memory intensive.

The parallel contact angle is plotted in Fig. 3(B) as a function of α for different absolute dry stripe widths. As outlined previously [1] the contact angle in the parallel direction is expected to follow the Cassie–Baxter equation

$$\cos\left(\theta_\parallel\right) = \frac{\cos\left(\theta_{wet}\right) + \alpha\cos\left(\theta_{dry}\right)}{1+\alpha} \tag{8}$$

The black line in Fig. 3(B) represents a calculation using equilibrium contact angles $\theta_{wet} = 40^\circ$ and $\theta_{dry} = 110^\circ$, identical to the values used for the simulations. As expected, the simple Cassie–Baxter model (Eq. (8)) is in agreement with the simulation results, except for the smallest dry stripe widths, which show a clear deviation from the black line.

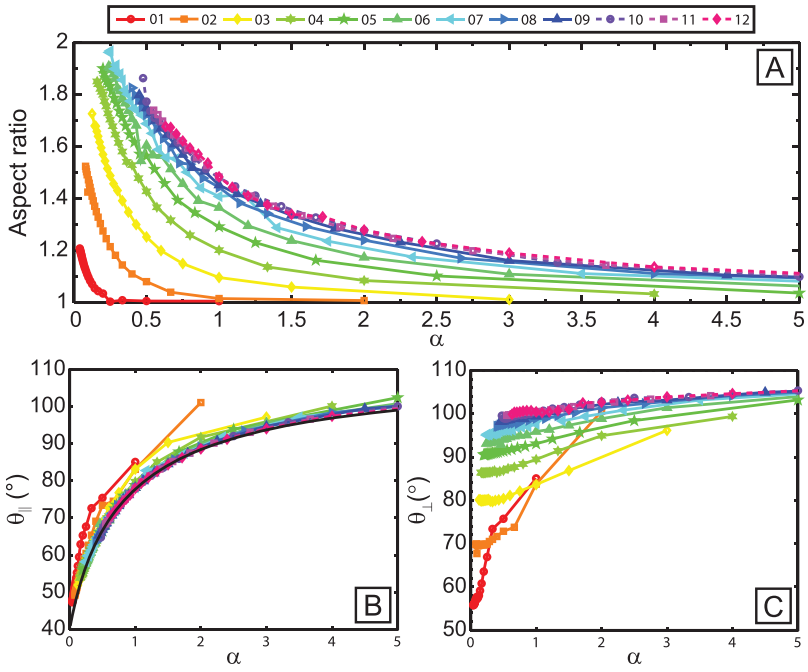

Fig. 3. Results of LBM simulations showing the droplet aspect ratio (A) as well as parallel (B) and perpendicular (C) contact angles as a function of α for different absolute dry stripe widths. The legend above the figure indicates the dry stripe widths used (in lattice units). The black line in (B) represents to Cassie–Baxter model with contact angles of $\theta_{wet} = 40^\circ$ and $\theta_{dry} = 110^\circ$, identical values as those used for the simulations.

The perpendicular contact angle is plotted in Fig. 3(C) as a function of α and the absolute dry stripe widths. Clearly, the perpendicular contact angle depends on both variables; the angle is low for the smallest dry stripe widths and larger for wider stripes. A small variation in the contact angle is found as a function of α, leading to slightly lower values for low α values. However the absolute dry stripe width has a more pronounced effect on the perpendicular contact angle. For large stripe widths the lines for the perpendicular contact angle collapse onto a single curve, very similar to the aforementioned trend observed for the aspect ratio.

In order to further investigate the dependence of the aspect ratio on the absolute stripe widths, we now focus on striped patterns with a fixed value $\alpha = 1.00$. From the experimental results, and also on the basis of simulations using Surface Evolver [36], we would not expect a large variation of the aspect ratio when varying the absolute stripe widths. In Fig. 4(A) the aspect ratio is plotted as a function of the absolute stripe widths of both stripes ($\alpha = 1.00$, so the stripes have equal widths). The aspect ratio is not constant, but depends on the absolute stripe widths. For small stripe widths the aspect ratio is close to one and as the stripe widths increase the aspect ratio also rises until it saturates at a value of 1.49 for stripe widths of 10–12 l.u.

In Fig. 4(B) the parallel and perpendicular contact angles are plotted as a function of the absolute stripe widths. The perpendicular contact angle shows the same trend as the aspect ratio; for low absolute stripe widths the contact angle is low, and it increases as the absolute stripe widths are increased, until the contact angle saturates at a value of 100°. The contact angle in the perpendicular direction approaches the contact angle on the dry stripe ($\theta_{dry} = 110^\circ$) but never reaches it, very similar to experimental observations and also SE simulations. This can be explained by the volume rearrangement in the droplets. A droplet deposited on a pristine 'dry' (lyophobic) surface will adopt a spherical shape with the contact angle that is set for the dry stripe. However, in the case of our chemically striped patterned surfaces the droplet will become elongated, stretching the droplet and therewith decreasing its height, lowering the perpendicular contact angle, as already discussed by Bliznyuk et al. [1].

The contact angle in the parallel direction is low and equal to the perpendicular angle for the smallest absolute stripe widths. As the stripe widths are increased the parallel and perpendicular contact angles start to differ, lowering the contact angle in the parallel direction and increasing the contact angle in the perpendicular direction. As the absolute stripe widths are increased further the parallel contact angle saturates at 78°, which is consistent with the modified Cassie–Baxter equation (Eq. (8)).

As outlined in our previous work [3] and is well-known in LBM simulations [38], the interface between the two phases is not sharp, but diffusive. The transition from the fluid density to the air density occurs over several lattice sites. In our case the interface spans about 6 lattice units, so a stripe that has a width less than this interface width is not as clearly felt as a wider stripe, leading to different contact angles on the surface. This effect can be clearly seen for the most narrow stripes considered in our simulations, i.e. 1–3 l.u. The contact angles are close to 90° and decrease slightly for larger stripes widths. This effect has previously also been reported by other groups [39,20]

Going back to the perpendicular contact angle in Fig. 3(C), the effect of the interface width is clearly observed. As the width of the stripes increases, the contact angle in the perpendicular direction also increases over the entire range of α values. The contact angle in the parallel direction approximates the black line for lower stripe widths while the perpendicular contact angle does not saturate, since both the dry and wet stripes have an influence on the parallel contact angle and only the dry stripe has an influence on the perpendicular contact angle. Due to the additional volume the height of a droplet becomes larger, while the contact line is pinned at the dry stripe leading to a higher perpendicular contact angle as a function of time. During this process the contact line will move slightly over the dry stripe. For small stripe widths it is easier to reach a wet stripe, since the width that needs to be crossed is lower, resulting in a lower maximum contact angle in the direction perpendicular to the stripes. In other words, the pinning force is not sufficiently strong to hold the droplet in place.

Similarly, the aspect ratio is low for small dry stripe widths as the dry stripe is more easily crossed. During growth the width of the

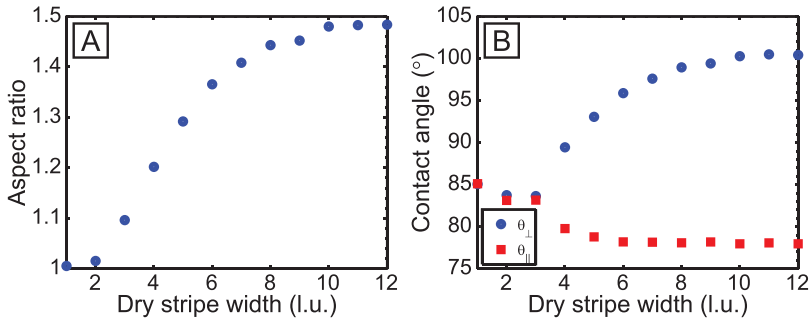

Fig. 4. (A) The aspect ratio of droplets simulated with LBM on patterns with α=1.00, but for varying absolute stripe widths. (B) The contact angles as a function of the stripe widths; blue circles and red squares represent perpendicular and parallel contact angles, respectively. (For interpretation of the references to color in this figure legend, the reader is referred to the web version of this article.)

droplet remains approximately constant while the height and the length both increase as a function of time, leading to larger aspect ratios. However, for small dry stripe widths this process cannot continue indefinitely, since the contact line will start to move over the dry stripe. As the dry stripe width is increased the aspect ratio goes up, since it takes longer to cross the dry stripe. Once the pinning force is large enough, for stripe widths from 10 l.u. and onwards, the maximum perpendicular contact angle does not change with wider dry stripes. Once this occurs the aspect ratio becomes independent of the dry stripe width. It is only a function of the ratio α as experienced by the collapse of the lines on a single curve.

4. Comparing LBM and SE simulations

The way in which droplet growth is implemented in the LBM simulations is very comparable to the multi-drop deposition we used to investigate the effect of deposition kinetics [5]; in both cases the contribution of kinetic energy to the final shape is negligible. This enables us to compare the lattice Boltzmann simulations to Surface Evolver results; the latter were done with the same contact angles as in the LBM simulations. The SE and LBM results for dry stripe widths >9 l.u. are plotted in Fig. 5, in terms of the aspect ratio (A) and contact angles (B) as a function of α.

The agreement in aspect ratio between the SE and LBM simulations is good, especially for large α values. As α becomes smaller the LBM results start to deviate from the SE results, which can be explained in terms of the contact angles. Both in the SE and LBM simulations the parallel contact angle is in agreement with the Cassie-Baxter model (Eq. (8); black line in Fig. 5(B)). The perpendicular contact angle shows a pronounced difference between the SE and LBM simulations. For surfaces with large α values they agree well with each other, as does the aspect ratio. For smaller α values the LBM perpendicular contact angle decreases while the SE angle increases, which causes a slight deviation in the aspect ratio. Notice that, as already indicated above, the perpendicular contact angle never reaches the contact angle as defined on the dry stripe.

Previously, we developed a simple geometrical model to describe the α-dependent aspect ratio as a function of parallel and perpendicular contact angles [36]. In Fig. 5(A) we compare results from this model with the numerical simulations. The parallel contact angle is identical for both, but the perpendicular contact angle is slightly different. The red curve is obtained using a perpendicular contact angle of 103° while the blue curve is plotted using a contact angle of 100°. For low aspect ratios the red curve is a better approximation, since the perpendicular angles are equal to 103°. However, for the high aspect ratios the blue curve fits better with the LBM simulations and the red curve fits better with the SE simulations, which is due to the small differences in the perpendicular contact angle.

We note that the number of wetted stripes in the two simulation methods is not the same; in the LBM simulations 7 stripes are wetted, while in the SE simulations 29 stripes are covered. However the results are comparable and the previously proposed model fits the data well. This shows that the droplet profiles in both the parallel and perpendicular direction can be approximated by a circular shape.

4.1. Varying stripe wettabilities for fixed α

Using both SE and LBM we also studied the dependence of droplet aspect ratio and contact angles as a function of the wettabilities of the stripes for a fixed stripe width ratio, i.e. α = 1.00. The absolute stripe widths for the LBM simulations were set to 10 l.u., since it allows for a relatively small lattice size, while the stripes are still larger than the interface width, resulting in an aspect ratio that is not dependent on the absolute stripe widths. The simulated contact angles range from 30° to 110°. In the lattice Boltzmann method used in this work it is difficult to obtain accurate contact angles close to 0° or 180°, therefore a lower limit of 30° is taken. [31]. The upper limit of the contact angle is set to 110°, since larger contact angles are experimentally not achievable on flat chemically modified surfaces.

In Fig. 6(A) the droplet aspect ratio is shown as a function of the contact angle of the wet stripe for SE (squares) and LBM (circles) simulations. The dry angles are indicated in the legend of the figure, ranging form 40° to 110°. The difference in wettability between the stripes is lower for higher wet contact angles, leading to lower aspect ratios.

Léopoldès and Bucknall [40] studied the effect of wettability contrast on sessile droplets on microstriped surfaces. They observed that droplets were highly elongated, slightly elongated, and close to spherical for high, intermediate and low wettability contrasts, respectively. In our calculations the same trend is observed. For high wettability contrast the aspect ratio is large, while for low wettability contrast a droplet is close to spherical. Both the SE and LBM simulations show the same trend, an almost linear decrease in aspect ratio as the wet contact angle is increased.

The macroscopic contact angles $\theta_{\parallel}$ and $\theta_{\perp}$ are plotted in Fig. 6(B,C) as a function of the wettability of the wet stripe, defined by their contact angle values. The parallel contact angle shows only a slight difference between the two simulation methods and agree well with the modified Cassie–Baxter equation, as shown by the solid lines in Fig. 6(B). The LBM simulations deviate slightly more from these lines, especially for larger contact angles. The volume of the droplet rises upon increasing the density in the droplet, which causes a slight overall density increase as a function of simulation time. For surfaces having large contact angles the droplets were grown for a longer time as compared to droplets deposited on lower contact angle surfaces, resulting in a denser droplet. The effective

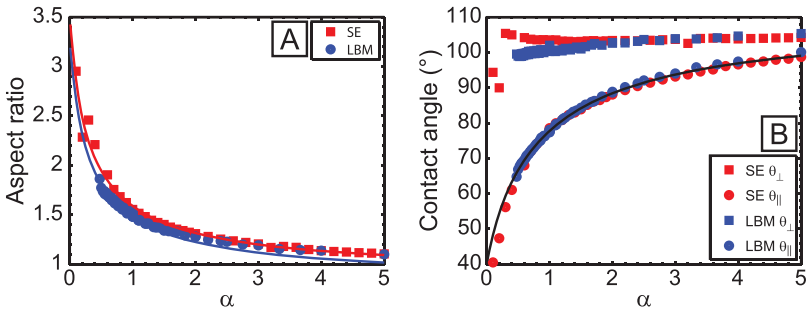

Fig. 5. (A) Aspect ratio of the simulated droplets as a function of α for the SE (red squares) and LBM (blue circles) simulations with dry stripe widths of at least 10 l.u. The solid lines represent the geometrical model (see text for details) with alternative perpendicular contact angles; for the red curve $\theta_\perp = 103^\circ$ and for the blue curve $\theta_\perp = 100^\circ$. (B) The contact angles as a function of α, both for the parallel and perpendicular direction. The black line represents the modified Cassie–Baxter model (Eq. (8)) with input angles $\theta_{wet} = 40^\circ$ and $\theta_{dry} = 110^\circ$. (For interpretation of the references to color in this figure legend, the reader is referred to the web version of this article.)

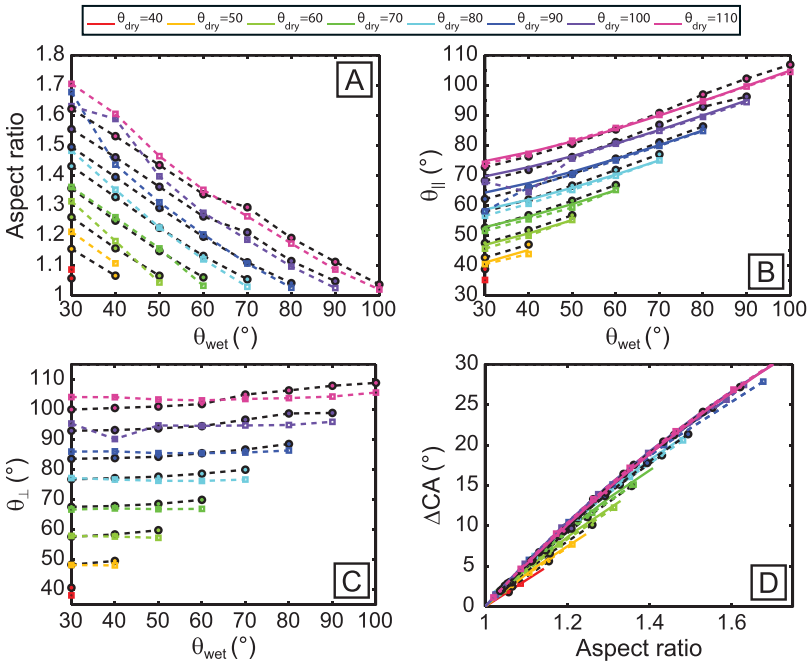

Fig. 6. (A) Aspect ratio as a function of θ_{wet} and θ_{dry} (the latter indicated by different colors); empty squares represent SE simulations and filled circles the LBM simulations. Parallel (B) and perpendicular (C) contact angles as a function of θ_{wet}; the solid lines (B) indicate the modified Cassie–Baxter equation. (D) The difference between perpendicular and parallel contact angles as a function of aspect ratio; the solid line represents a model calculation (see text for details [36]).

contact angles of the stripes come closer to 90° as the density is higher, resulting in a slightly higher contact angle for the parallel direction [31].

The contact angles in the perpendicular direction plotted in Fig. 6(C) are slightly lower than the θ_{dry} values, due to the aforementioned volume rearrangement. The contact angles for the LBM simulations show a slight increase as θ_{wet} increases. As mentioned before the wettability contrast decreases for larger θ_{wet} leading to lower aspect ratios and therefore less volume rearrangement, resulting in higher perpendicular contact angles. The SE simulations do not show this trend, since the perpendicular contact angle is completely independent of θ_{wet}. The small differences in both the parallel and perpendicular contact angles result in a slight difference between the aspect ratios obtained using the two simulation techniques.

In Fig. 6(D) the difference between $\theta_\perp$ and $\theta_\parallel$ is plotted as a function of the aspect ratio, both for the SE and LBM simulations. The curves seem to collapse onto a single curve, however points corresponding to lower θ_{dry} are systematically lower than points corresponding to a higher θ_{dry}. Using the aforementioned basic geometrical model [36] the difference in contact angles can be calculated as a function of aspect ratio; results are represented by the colored solid lines in Fig. 6(D). The solid lines are in perfect agreement with the data indicating that both sides of the droplet can be approximated by a spherical cap. The aspect ratio therefore not only depends on the difference between the contact angles, but also on the absolute value of the contact angles, as seen in Eq. (8). A very similar trend as observed in Fig. 6(D) was also reported by Semprebon and co-workers for anisotropic water droplets on single rectangular posts [41].

5. Wetting of a single stripe

In the simulations as described in this work and also in recently reported experiments [5,3,29,42], droplets deposited on chemically stripe-patterned surfaces exhibit a highly elongated shape for low α values. However, experimentally it is not straightforward to achieve very low α values. Values for α approaching zero imply that the dry stripes become very narrow. A droplet deposited on such a surface would easily pass these stripes, due to kinetic effects described previously [5], resulting in an almost spherical shape. This effect can also be observed in the LBM simulations

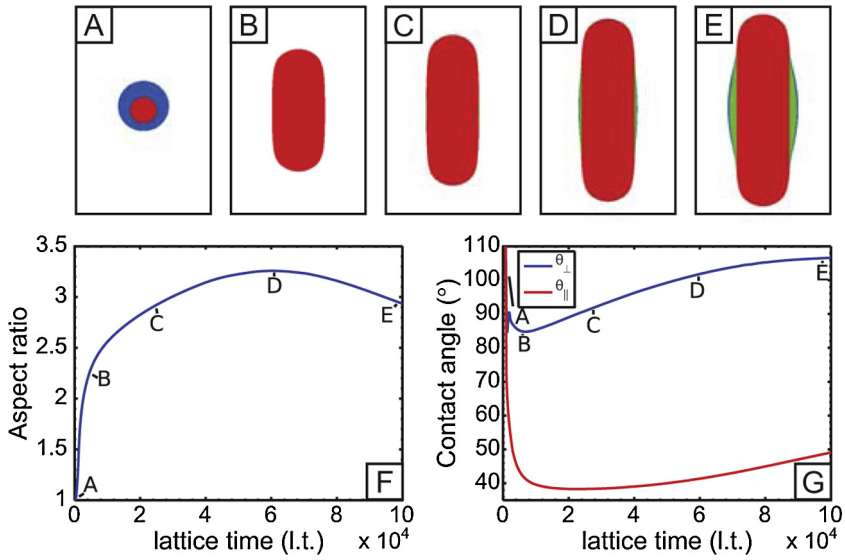

Fig. 7. LBM simulation of wetting a single stripe having a width of 45 lattice units. (A–E) Snapshots 'viewing' the droplets from the bottom. Different colors are used to distinguish between the liquid–vapour interface (blue), the liquid–solid interface for the wet stripe (red) and the liquid–solid interface for the dry stripes (green). Initially, the droplet is a sphere and starts to elongate on the stripe, eventually reaching a bulge state (D–E). Aspect ratio (F) and contact angles (G) as a function of lattice time; the letters indicate the moments at which the different snapshots were taken. (For interpretation of the references to color in this figure legend, the reader is referred to the web version of this article.)

as performed for this paper. For dry stripe widths of 1 l.u. the aspect ratio is considerably smaller than for large stripe widths (see Fig. 4), which would also happen in the experiments if the dry stripe widths become too small.

The contact angle in the parallel direction can be calculated using the Cassie–Baxter model (Eq. (8)) for α values approaching zero. In this case, the contact angle in the parallel direction becomes equal to the contact angle on the wet stripe. If there is sufficient pinning on the dry stripes, the contact angle in the perpendicular direction will approach the contact angle on the dry stripe. This situation is analogous to wetting of a single wet stripe confined by two infinitely wide dry stripes. Kusumaatmaja et al. [6,8] already showed that droplet dynamics can be modeled on single stripes using the lattice Boltzmann approach. They focused on the dynamics of the morphology transitions between multiple stripes, and not on the maximum aspect ratio that can be achieved.

As for the previous simulations, we deposit a droplet onto the surface and we let it grow by increasing the density of the droplet. In Fig. 7 the evolution of the droplet shape is shown (A–E). Also, the time evolution of the aspect ratio (F) and contact angles (G) of a droplet deposited on a wet stripe is shown. The initial radius of the droplet is set to be half of the stripe width (45 l.u.). (A) At the start of the simulation, a spherical drop is placed on the surface. The colors of the snapshots indicate the liquid–vapor interface (blue), the liquid wetting the wet stripe (red), and the liquid wetting the dry stripes (green). (B) The droplet has spread towards the boundary between wet and dry stripes and its shape becomes elongated. The perpendicular contact angle has decreased and the parallel contact angle adopts the value that was set for the wet stripe. (C) As more volume is added the droplet starts to elongate substantially. The contact angle in the perpendicular direction becomes larger than 90° and a bulge starts to form, partially wetting the dry stripes. (D) The droplet is in the bulge state and the maximum aspect ratio is reached. From the contact angle values it is difficult to determine when the maximum aspect ratio is reached. Close to the time of maximum aspect ratio both the parallel and perpendicular contact angles are increasing as a function of time, and at point (D) they amount to $\theta_{\parallel} = 41.4°$ and $\theta_{\perp} = 100.8°$. After this point the width of the droplet starts to increase more (due to bulging) than the length of the droplet, resulting in lower aspect ratios as time continues until the end of the simulation (E).

Gau et al. [12] and Brinkmann et al. [14,43,15] studied the shape of a droplet wetting a single stripe, and they have identified different shape regimes for a contact angle of 130° on the dry stripes: (i) a spherical cap, not touching the boundary between the stripes with a contact angle of the wet stripe, (ii) an extended channel is formed with free moving end caps, (iii) the droplet undergoes a morphological transition from the channel state to the bulge state once the perpendicular contact angle is 90°. In our case we observe similar shapes. Regime (i) is skipped due to the large volume already present at the start of the simulation, i.e. the droplet becomes elongated as soon as it has spread over the surface. For snapshots (B, C) the droplet is elongated and the length of the channel starts to increase, corresponding to regime (ii). Snapshots (D, E) show the droplet in the bulge state corresponding with regime (iii). Brinkmann and Lipowsky [14] have done calculations to determine which state (channel or bulge) is preferred, but they did not focus on the maximum aspect ratio that can be achieved. The bulge state becomes preferential once the contact angle in the perpendicular direction exceeds 90°, so it depends on the height of the droplet as a function of the stripe width.

We also investigate the influence of the absolute stripe widths (in the range 10–60 l.u.) on the maximum aspect ratio that is achieved. The result is plotted in Fig. 8 together with the directional contact angles as a function of the wet stripe width. There is an influence of the absolute stripe width on the aspect ratio, just as in the case of a droplet wetting 7 stripes (Fig. 3). The maximum aspect ratio clearly increases for wider stripes, to eventually saturate at a value of approximately 3.2–3.3. For the widest stripes the aspect ratio decreases slightly, which can be ascribed to the actual contact angles values. The contact angles in the parallel direction continuously decreases as the wet stripe width is increased, eventually reaching the value that was set for the wet stripe. The perpendicular contact angles also decrease as a function of stripe widths, due to the aforementioned rearrangement of volume and larger density of the droplet.

The maximum aspect ratio achieved is in reasonable agreement with the simple model that was proposed previously [36]. In this

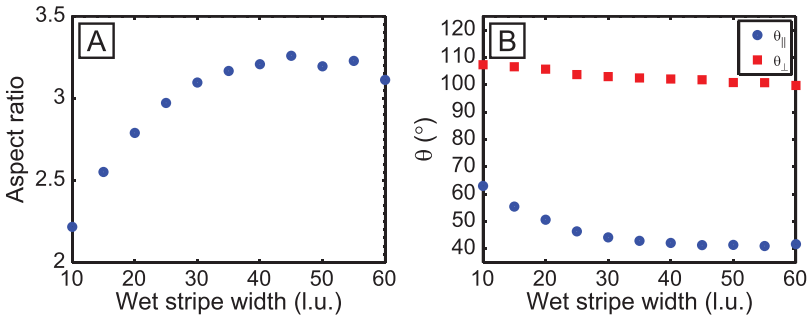

Fig. 8. (A) The maximum aspect ratio that is achieved as a function of the wet stripe width for single stripe wetting. The aspect ratio increases as the wet stripe width is increased. (B) The corresponding perpendicular (red squares) and parallel (blue circles) contact angles as a function of the wet stripe width. For large stripe widths the parallel contact angle approximates the contact angle that was set for the wet stripe. (For interpretation of the references to color in this figure legend, the reader is referred to the web version of this article.)

case $\theta_{\parallel}$ can be set to the contact angle on the wet stripe and $\theta_{\perp}$ can have a maximum value of 110°, leading to an aspect ratio of 3.92. From all the simulations that we have done, we always find that the perpendicular contact angle is slightly lower than the contact angle on the corresponding stripe. If we set the perpendicular contact angle to 100° we obtain an aspect ratio of 3.27 which is very close to the values from the simulations in Fig. 8(A).

Inspired by the work of Lipowsky et al. [15], we plotted the scaled volume as a function of the parallel contact angle (A), the perpendicular contact angle (B) and the aspect ratio (C). The result is shown in Fig. 9. The volume is scaled to the cube of the wet stripe width, given by $V/(W_{\text{wet}})^3$. For low volumes at the first stage of the simulation, the droplet is deposited on the stripe starting with large contact angles which rapidly decrease due to spreading. Upon increasing the volume the contact angles decrease until they reach the value that is set for the wet stripe. Here the influence of the absolute stripe width can also be observed; wider stripes exhibit lower contact angles. The contact line is close to the boundary of the dry stripes, making it difficult to advance further on the stripe. Once the perpendicular contact angle reaches an angle that exceeds 90° the droplet starts to grow in the bulge state. The parallel contact angles rapidly increase in agreement with the work of Lipowsky et al. [43,15]. For even large volumes the parallel contact angle increases far beyond the contact angle that is set for the wet stripe, since the parallel side is now wetting both the wet and dry stripes.

As already mentioned, the perpendicular contact angle for low volumes in the initial stage of the simulation is large. Once the droplet has been deposited spreading gives rise to a rapid decrease of the contact angle, until a minimum is reached. Lower contact angles are reached for wider stripes since these droplets are more elongated. As the volume increases the contact angles start to increase eventually approximating the contact angle on the dry stripe for large volumes; in this situation a large portion of the droplet is wetting the dry stripe.

As is clear from the curves in Fig. 9(C) the maximum achievable aspect ratio exhibits a pronounced dependence on the absolute stripe width. For the smallest volumes the droplets are deposited on the surface starting with an aspect ratio of unity. As the volume is increased the aspect ratio rises due to lateral confinement of the droplet, i.e. pinning of the contact line in the direction perpendicular to the stripes. At some point the aspect ratios reach a maximum, the value of which depends on the absolute stripe width. The volume at which the maximum aspect ratio is achieved is also a function of the stripe widths; for the smallest stripe width the scaled volume amounts to 2 when the maximum aspect ratio is reached, while for the widest stripe this occurs at a volume of 1.2. This effect can be understood by considering the parallel contact angle, which is lower for the same volume for larger stripe widths.

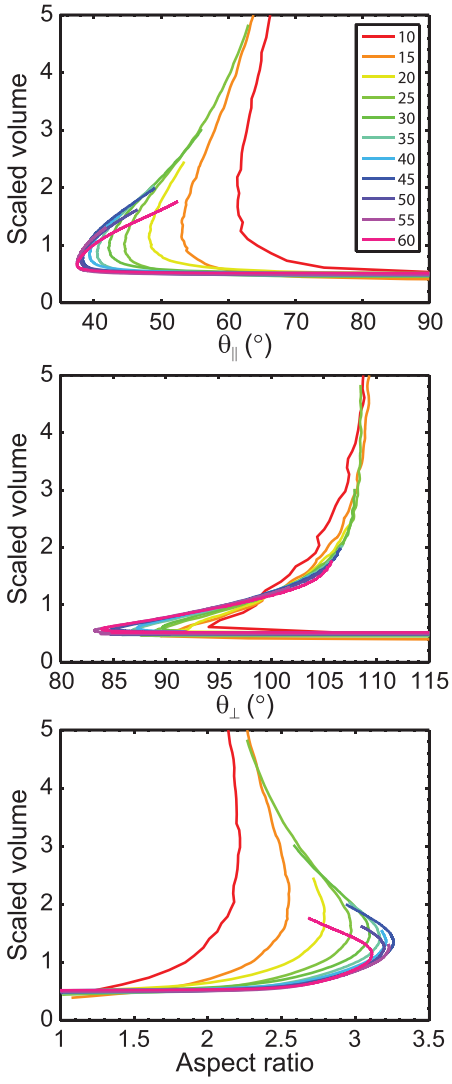

Fig. 9. The volume scaled to the wet stripe width as a function of the parallel contact angle (A), the perpendicular contact angle (B) and the aspect ratio (C). The legend indicates the wet stripe widths used.

6. Conclusions

We have presented the potential of lattice Boltzmann (LBM) simulations to model the kinetics involved in droplets on chemically stripe-patterned surfaces. The first example is that of an impacting droplet on these substrates with directional wetting

properties. Comparison of simulations to experimental results shows very good qualitative agreement in terms of the inertia in the impact event. Analysis in terms of the dimensionless Weber number reveals that the maximum spreading diameter has a profound influence on the final aspect ratio of the static droplets.

Additionally, single stripe wetting was also modeled using the LBM simulations, focusing on the maximum aspect ratio that can be achieved. The contact angle in the parallel direction approaches the contact angle on the wet stripe, and the contact angle in the perpendicular direction is slightly lower then the contact angle on the dry stripe. This determines the maximum aspect ratio that can be achieved, therewith finding the maximum aspect ratio as α approaches zero, in the limit of low kinetic energy and sufficiently large stripe widths.

To validate our LBM approach, we have performed a detailed comparison with Surface Evolver (SE) simulations for droplets deposited on chemically stripe-patterned surfaces. In the case of the LBM simulations the volume of the droplet is increased by increasing the density of the droplet. The maximum aspect ratios that droplets reach before wetting additional stripes depends not only on the ratio α of the widths of hydrophobic and hydrophilic stripes, but also on their absolute widths due to the diffusive interface. For large stripe widths, the effect of the diffusive interface can be neglected and the aspect ratio as a function of α collapses onto a single curve, independent of the absolute stripe widths. The LBM and SE simulations show the same trend in aspect ratio as a function of α; small differences can be contributed to a slight deviation in the perpendicular contact angle. Moreover, the simple model that was proposed in our previous work proves to be a good approximation for both simulation techniques. For surfaces with $\alpha = 1.00$ the wettabilities of the stripes were varied, resulting in different aspect ratios. Again, overall the SE and LBM simulations show very similar results. With LBM it is possible to study dynamics of the droplets, but it is more computational intensive than the SE simulations.

Acknowledgements

We thank all PIN group members for the available computational time on idle computers. This work is supported by NanoNextNL, a micro and nanotechnology consortium of the Government of the Netherlands and 130 partners. This work was sponsored by NWO Exacte Wetenschappen (Physical Sciences) for the use of supercomputer facilities, with financial support from the Nederlandse Organisatie voor Wetenschappelijk Onderzoek (Netherlands Organization for Scientific Research, NWO).

References

[1] O. Bliznyuk, E. Vereshchagina, E.S. Kooij, B. Poelsema, Scaling of anisotropic droplet shapes on chemically stripe-patterned surfaces, Phys. Rev. E 79 (2009) 041601, http://dx.doi.org/10.1103/PhysRevE.79.041601.
[2] O. Bliznyuk, H.P. Jansen, E.S. Kooij, B. Poelsema, Initial spreading kinetics of high-viscosity droplets on anisotropic surfaces, Langmuir 26 (9) (2010) 6328–6334, http://dx.doi.org/10.1021/la903205e.
[3] H.P. Jansen, K. Sotthewes, J. van Swigchem, H.J.W. Zandvliet, E.S. Kooij, Lattice Boltzmann modeling of directional wetting: comparing simulations to experiments, Phys. Rev. E 88 (2013) 013008, http://dx.doi.org/10.1103/PhysRevE.88.013008.
[4] B.B.J. Stapelbroek, H.P. Jansen, E.S. Kooij, J.H. Snoeijer, A. Eddi, Universal spreading of water drops on complex surfaces, Soft Matter 10 (2014) 2641–2648, http://dx.doi.org/10.1039/C3SM52464G.
[5] H.P. Jansen, K. Sotthewes, C. Ganser, C. Teichert, H.J.W. Zandvliet, E.S. Kooij, Tuning kinetics to control droplet shapes on chemically striped patterned surfaces, Langmuir 28 (37) (2012) 13137–13142, http://dx.doi.org/10.1021/la302551m.
[6] H. Kusumaatmaja, J. Léopoldès, A. Dupuis, J.M. Yeomans, Drop dynamics on chemically patterned surfaces, Europhys. Lett. 73 (5) (2006) 740.
[7] H. Kusumaatmaja, A. Dupuis, J.M. Yeomans, Lattice Boltzmann simulations of drop dynamics, Math. Comput. Simul. 72 (2–6) (2006) 160–164, http://dx.doi.org/10.1016/j.matcom.2006.05.016.
[8] H. Kusumaatmaja, J.M. Yeomans, Controlling drop size and polydispersity using chemically patterned surfaces, Langmuir 23 (2) (2007) 956–959, http://dx.doi.org/10.1021/la062082w.
[9] H. Kusumaatmaja, R.J. Vrancken, C.W.M. Bastiaansen, J.M. Yeomans, Anisotropic drop morphologies on corrugated surfaces, Langmuir 24 (14) (2008) 7299–7308, http://dx.doi.org/10.1021/la800649a.
[10] R. David, A.W. Neumann, Anisotropic drop shapes on chemically striped surfaces, Colloids Surf. A 32–36 (2012) 393.
[11] R. David, A.W. Neumann, Shapes of drops in the Cassie state on grooved surfaces, Colloids Surf. A 399 (2012) 41–45.
[12] H. Gau, S. Herminghaus, P. Lenz, R. Lipowsky, Liquid morphologies on structured surfaces: from microchannels to microchips, Science 283 (5398) (1999) 46–49, http://dx.doi.org/10.1126/science.283.5398.46.
[13] A.A. Darhuber, S.M. Troian, S.M. Miller, S. Wagner, Morphology of liquid microstructures on chemically patterned surfaces, J. Appl. Phys. 87 (11) (2000) 7768–7775, http://dx.doi.org/10.1063/1.373452.
[14] M. Brinkmann, R. Lipowsky, Wetting morphologies on substrates with striped surface domains, J. Appl. Phys. 92 (8) (2002) 4296–4306, http://dx.doi.org/10.1063/1.1506003.
[15] R. Lipowsky, M. Brinkmann, R. Dimova, T. Franke, J. Kierfeld, X. Zhang, Droplets, bubbles, and vesicles at chemically structured surfaces, J. Phys.: Condens. Matter 17 (9) (2005) S537.
[16] R. Lipowsky, M. Brinkmann, R. Dimova, C. Haluska, J. Kierfeld, J. Shillcock, Wetting, budding, and fusion-morphological transitions of soft surfaces, J. Phys.: Condens. Matter 17 (31) (2005) S2885.
[17] F. Mugele, A. Klingner, J. Buehrle, D. Steinhauser, S. Herminghaus, Electrowetting: a convenient way to switchable wettability patterns, J. Phys.: Condens. Matter 17 (9) (2005) S559.
[18] K. Khare, S. Herminghaus, J.-C. Baret, B.M. Law, M. Brinkmann, R. Seemann, Switching liquid morphologies on linear grooves, Langmuir 23 (26) (2007) 12997–13006, http://dx.doi.org/10.1021/la701899u.
[19] R. Seemann, M. Brinkmann, E.J. Kramer, F.F. Lange, R. Lipowsky, Wetting morphologies at microstructured surfaces, Proc. Natl. Acad. Sci. U. S. A. 102 (6) (2005) 1848–1852, http://dx.doi.org/10.1073/pnas.0407721102.
[20] F.J.M. Ruiz-Cabello, H. Kusumaatmaja, M.A. Rodríguez-Valverde, J.M. Yeomans, M.A. Cabrerizo-Vílchez, Modeling the corrugation of the three-phase contact line perpendicular to a chemically striped substrate, Langmuir 25 (14) (2009) 8357–8361.
[21] H. Kusumaatmaja, R. Lipowsky, Equilibrium morphologies and effective spring constants of capillary bridges, Langmuir 26 (24) (2010) 18734–18741, http://dx.doi.org/10.1021/la102206d.
[22] D. Ferraro, C. Semprebon, T. Tóth, E. Locatelli, M. Pierno, G. Mistura, M. Brinkmann, Morphological transitions of droplets wetting rectangular domains, Langmuir 28 (39) (2012) 13919–13923, http://dx.doi.org/10.1021/la302854t.
[23] H. Matsui, Y. Noda, T. Hasegawa, Hybrid energy-minimization simulation of equilibrium droplet shapes on hydrophilic/hydrophobic patterned surfaces, Langmuir 28 (2012) 15450–15453.
[24] A. Promraksa, L.J. Chen, Modeling contact angle hysteresis of a liquid droplet sitting on a cosine wave-like pattern surface, J. Colloid Interface Sci. 384 (2012) 172–181.
[25] N.T. Chamakos, M.E. Kavousanakis, A.G. Papathanasiou, Enabling efficient energy barrier computations of wetting transitions on geometrically patterned surfaces, Soft Matter 9 (2013) 9624–9632.
[26] R. Zheng, H. Liu, J. Sun, Y. Ba, Droplet hysteresis investigation on non-wetting striped textured surfaces: a lattice Boltzmann study, Phys. A 411 (2014) 53–62.
[27] H.S. Grewal, I.J. Cho, J.E. Oh, E.S. Yo, Effect of topography on the wetting of nanoscale patterns: experimental and modeling studies, Nanoscale 6 (2014) 15321–15332.
[28] G. Pashos, A. Kokkoris, A.G. Boudouvis, A modified phase-field method for the investigation of wetting transitions of droplets on patterned surfaces, J. Comput. Phys. 283 (2015) 4258–4270.
[29] H.P. Jansen, K. Sotthewes, C. Ganser, H. Zandvliet, C. Teichert, E.S. Kooij, Shape of picoliter droplets on chemically striped patterned substrates, Langmuir 30 (2014) 11574–11581.
[30] X. Shan, H. Chen, Lattice Boltzmann model for simulating flows with multiple phases and components, Phys. Rev. E 47 (1993) 1815–1819, http://dx.doi.org/10.1103/PhysRevE.47.1815.
[31] H. Huang, D.T. Thorne, M.G. Schaap, M.C. Sukop, Proposed approximation for contact angles in Shan-and-Chen-type multicomponent multiphase lattice Boltzmann models, Phys. Rev. E 76 (2007) 066701, http://dx.doi.org/10.1103/PhysRevE.76.066701.
[32] M.C. Sukop, D.T. Thorne Jr., Lattice Boltzmann Modeling an Introduction for Geoscientists and Engineers, Springer-Verlag, Berlin, Heidelberg, 2006.
[33] R. Cornubert, D. d'Humires, D. Levermore, A Knudsen layer theory for lattice gases, Phys. D 47 (1991) 241–259.
[34] D.P. Ziegler, Boundary conditions for lattice Boltzmann simulations, J. Stat. Phys. 71 (1993) 1171–1177.
[35] K.A. Brakke, Surface Evolver manual version 2. 30, 2008.
[36] H.P. Jansen, O. Bliznyuk, E.S. Kooij, B. Poelsema, H.J.W. Zandvliet, Simulating anisotropic droplet shapes on chemically striped patterned surfaces, Langmuir 28 (1) (2012) 499–505, http://dx.doi.org/10.1021/la2039625.
[37] C. Clanet, C. Béguin, D. Richard, D. Quéré, Maximal deformation of an impacting drop, J. Fluid Mech. 517 (2004) 199–208, http://dx.doi.org/10.1017/S0022112004000904.

[38] D.M. Anderson, G.B. McFadden, A.A. Wheeler, Diffuse-interface methods in fluid mechanics, Annu. Rev. Fluid. Mech. 30 (1998) 139–165.
[39] D. Iwahara, H. Shinto, M. Miyahara, K. Higashitani, Liquid drops on homogeneous and chemically heterogeneous surfaces: a two-dimensional lattice Boltzmann study, Langmuir 19 (21) (2003) 9086–9093, http://dx.doi.org/10.1021/la034456g.
[40] J. Léopoldès, D.G. Bucknall, Droplet spreading on microstriped surfaces, J. Phys. Chem. B 109 (18) (2005) 8973–8977, http://dx.doi.org/10.1021/jp0508094.
[41] C. Semprebon, G. Mistura, E. Orlandini, G. Bissacco, A. Segato, J.M. Yeomans, Anisotropy of water droplets on single rectangular posts, Langmuir 25 (10) (2009) 5619–5625, http://dx.doi.org/10.1021/la8041742.
[42] H.P. Jansen, H. Zandvliet, E.S. Kooij, Evaporation of elongated droplets on chemically stripe-patterned surfaces, Int. J. Heat Mass Transf. 82 (2015) 537–544.
[43] R. Lipowsky, Morphological wetting transitions at chemically structured surfaces, Curr. Opin. Colloid Interface Sci. 6 (1) (2001) 40–48, http://dx.doi.org/10.1016/S1359-0294(00)00086-8.